Science Advances

Supplementary Materials for

Large-scale smart bioreactor with fully integrated wireless multivariate sensors and electronics for long-term in situ monitoring of stem cell culture

Jimin Lee *et al.*

Corresponding author: Woon-Hong Yeo, whyeo@gatech.edu; Young Charles Jang, young.jang@emory.edu

The PDF file includes:

Figs. S1 to S33
Tables S1 to S8
Legends for movies S1 to S3

Other Supplementary Material for this manuscript includes the following:
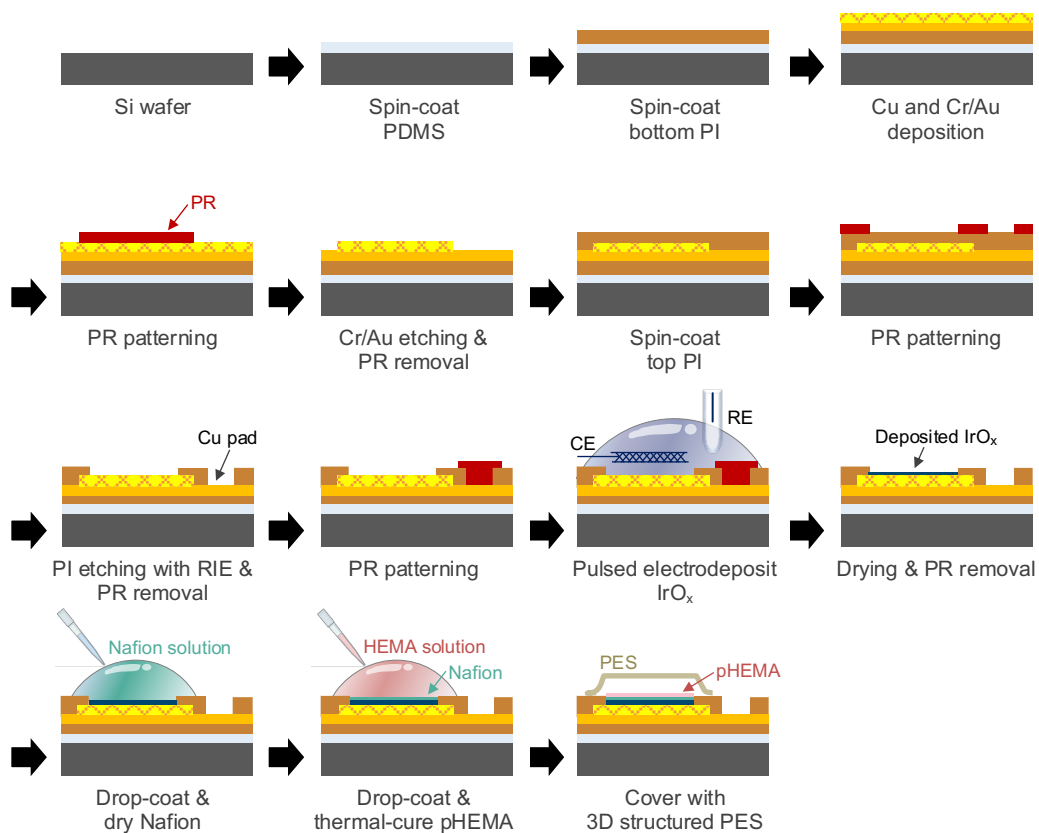
Movies S1 to S3

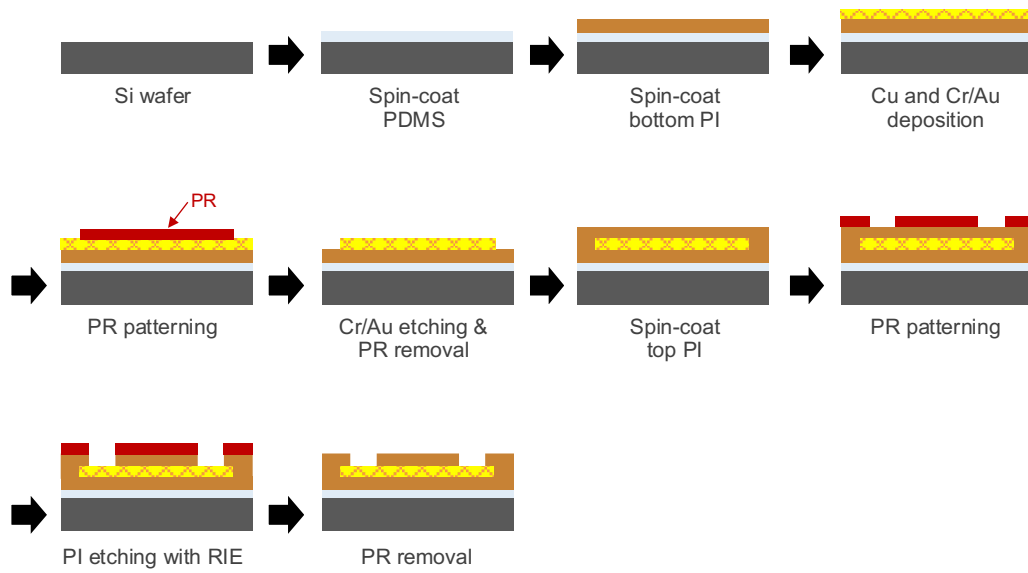**Fig. S1. Schematics illustration of thin-film pH sensor fabrication.**

Fig. S2. Schematics illustration of thin-film temperature sensor fabrication.
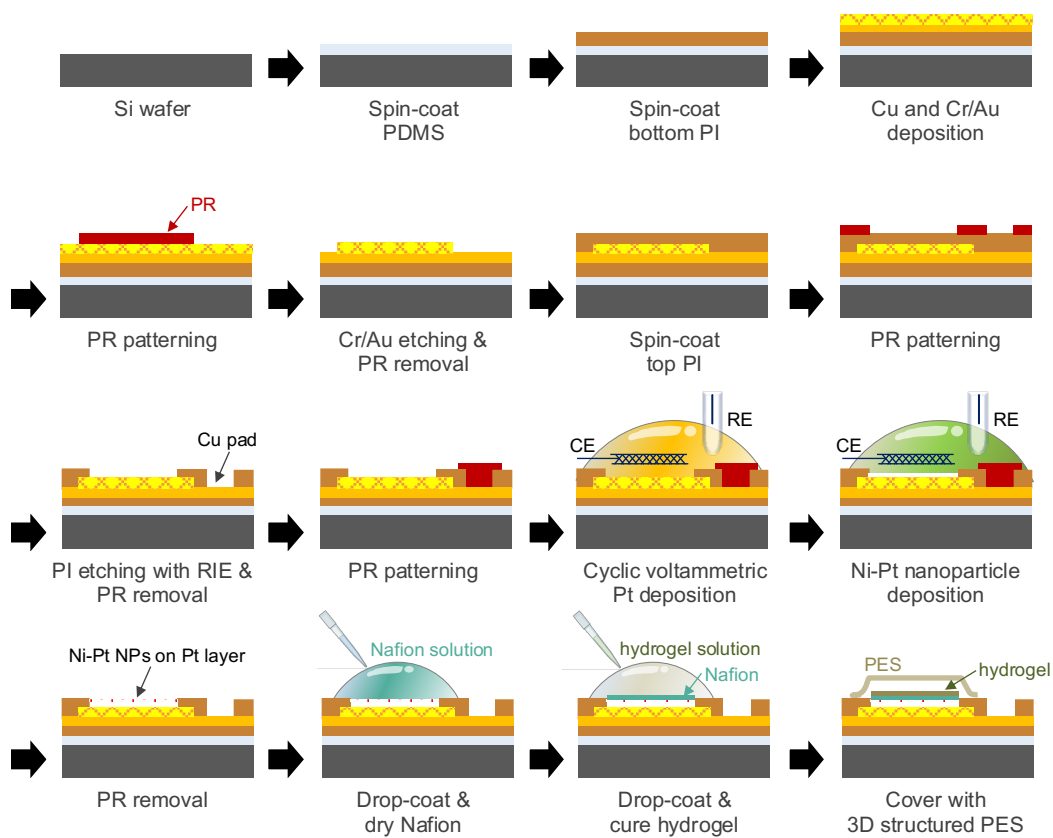
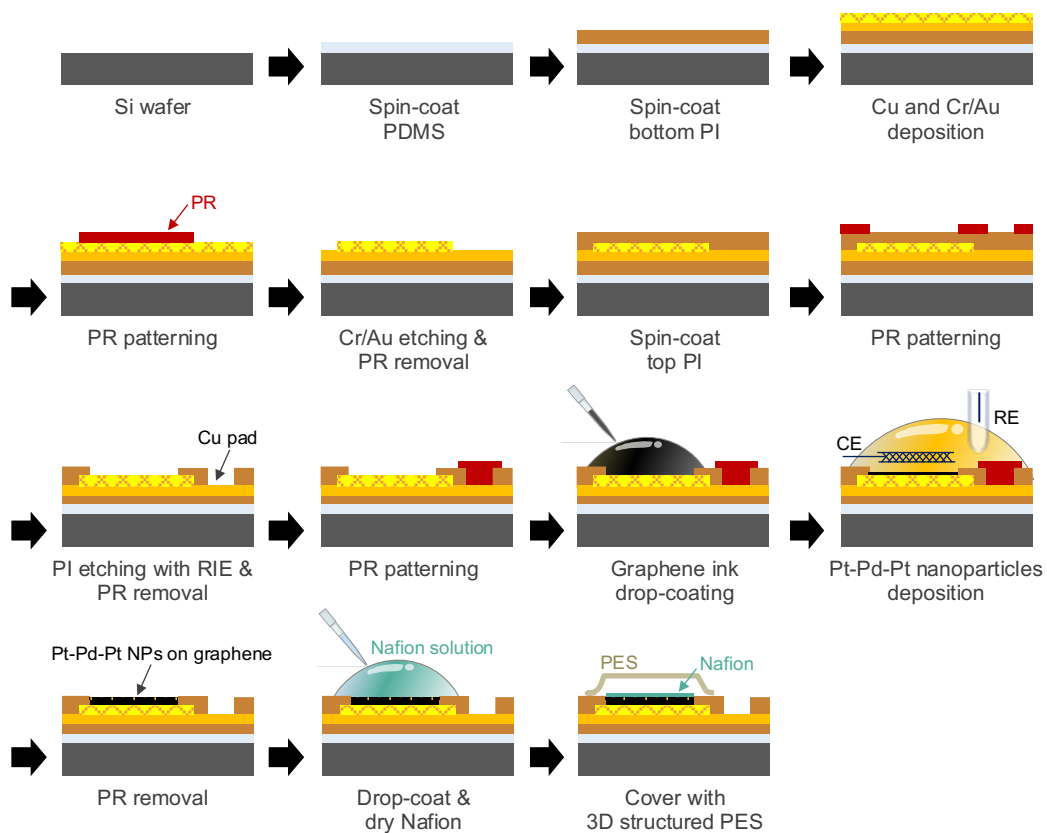**Fig. S3. Schematics illustration of thin-film dissolved oxygen sensor fabrication.**

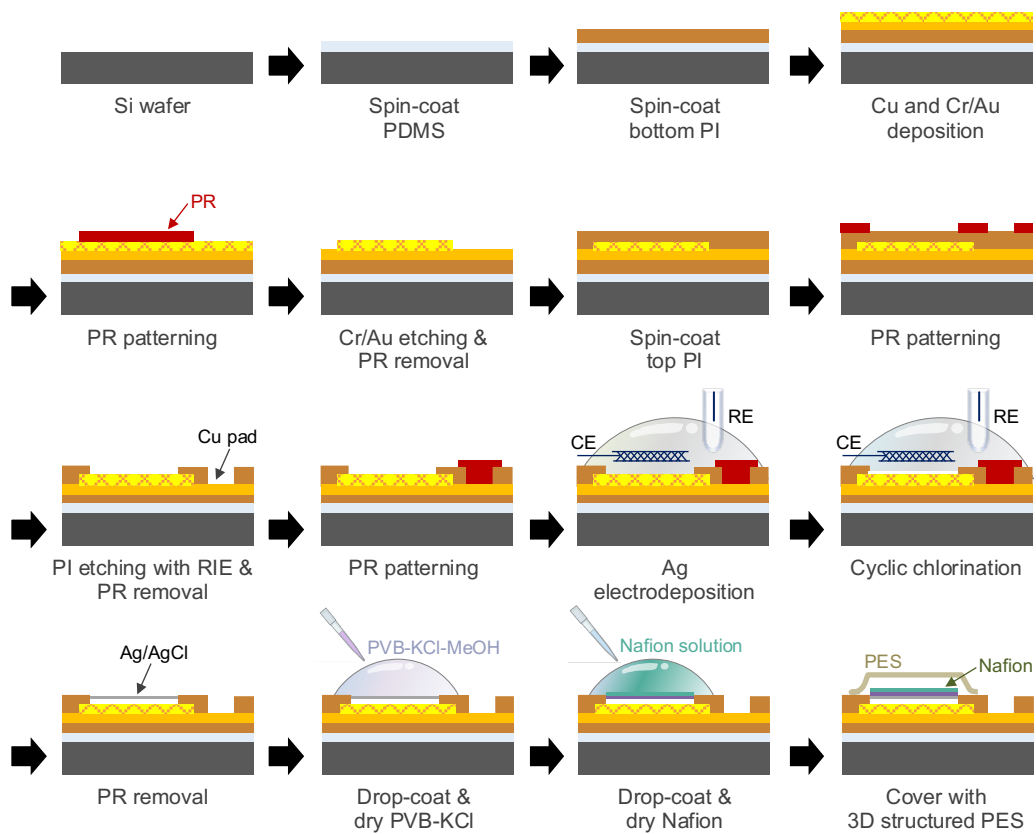**Fig. S4. Schematics illustration of thin-film glucose sensor fabrication.**

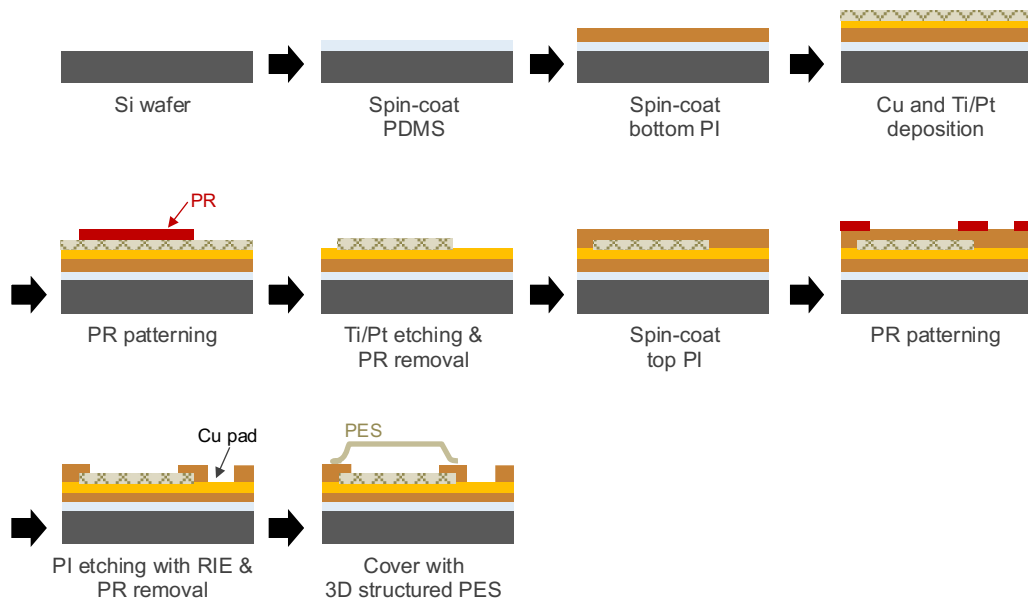**Fig. S5. Schematics illustration of thin-film reference electrode fabrication.**

Fig. S6. Schematics illustration of thin-film counter electrode fabrication.

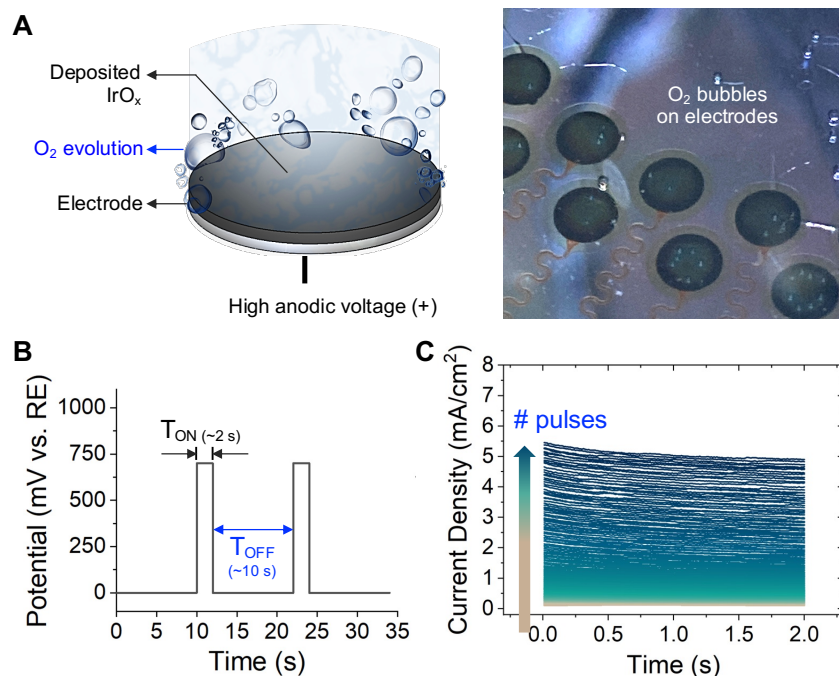**Fig. S7. Optimized IrO$_x$ deposition. a Schematic illustration of the electrode surface during deposition of IrO$_x$ for pH sensor fabrication. (A)** photograph taken during electrodeposition is shown at the right. **(B)** Voltage waveform of the pulsed electrodeposition for a uniform result on sensor surface. **(C)** Change in current density with the increased number of pulses.
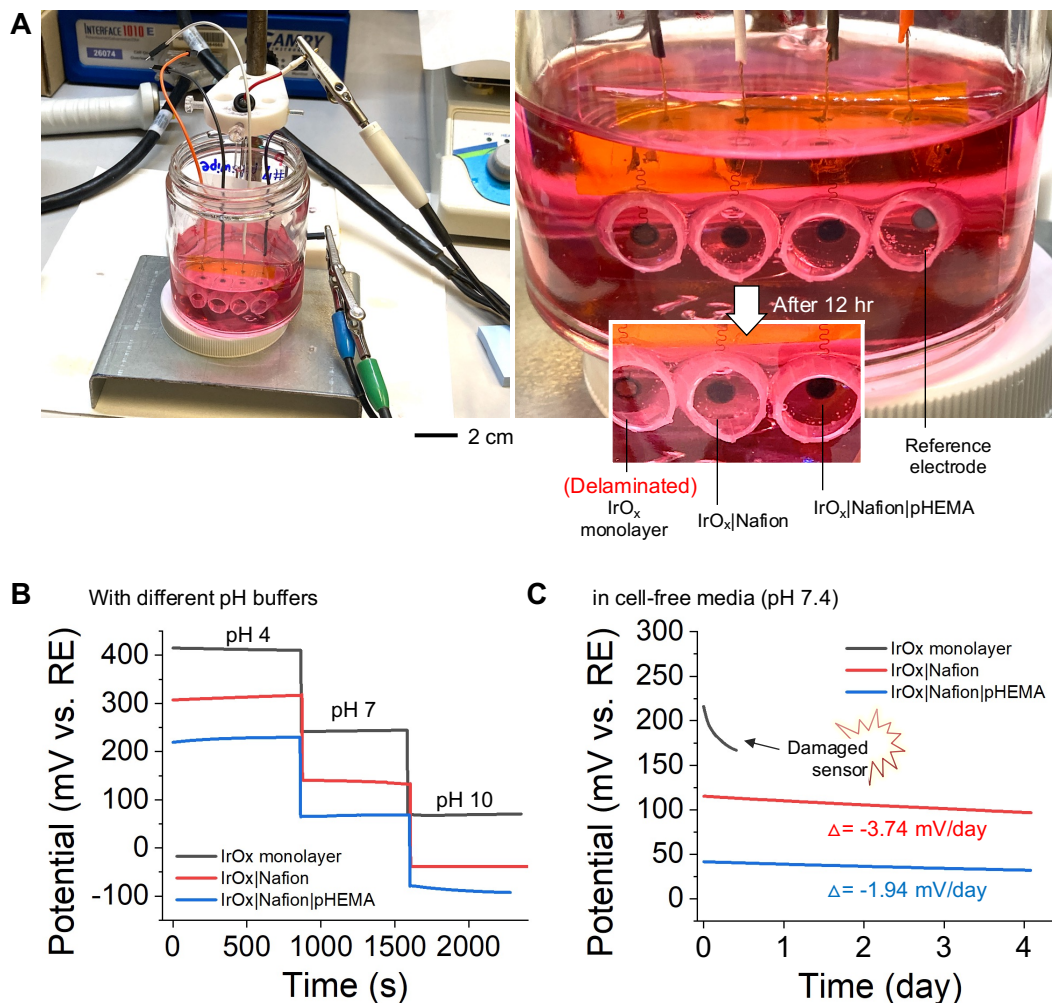
Fig. S8. Sensing performance of pH sensors with various membranes on IrO$_x$ monolayer. (A) Experimental setup for a pH sensor evaluation with Gamry potentiostat under different pH buffers for continuous 4 days. **(B)** Voltage response of each pH sensors with different pH buffers (e.g., pH 4, 7, 10 solutions). **(C)** Long-term stability evaluation for 4 days.
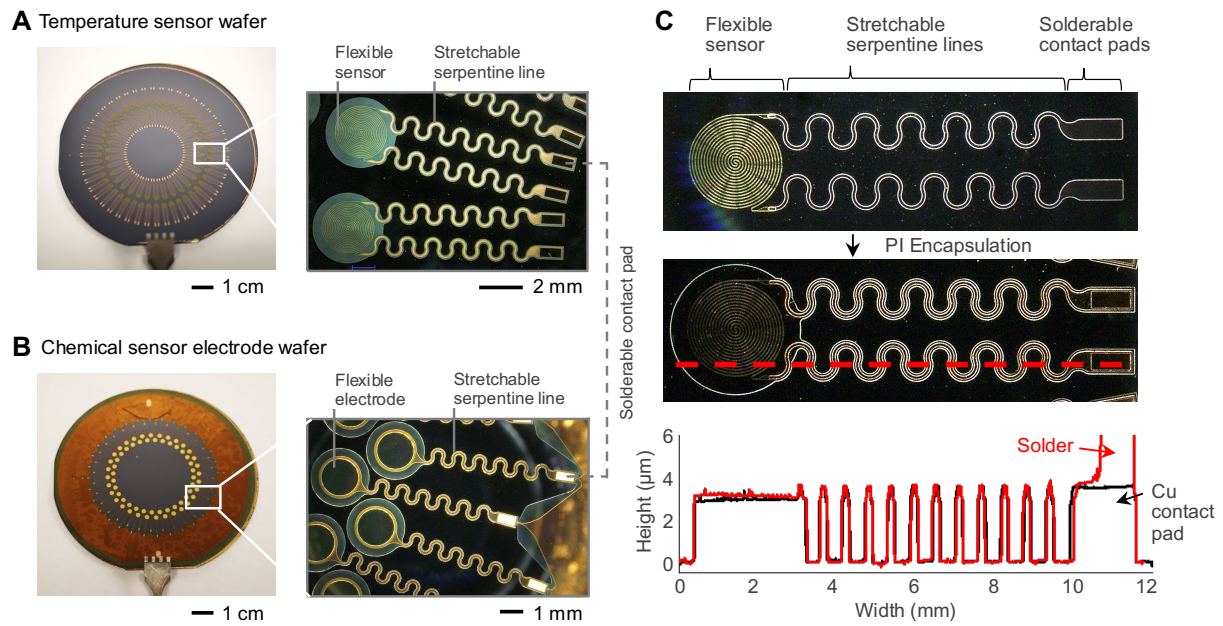
Fig. S9. Wafer-scale bare thin-film sensor and their main features. (A) Temperature sensor. **(B)** Chemical sensor electrode wafer. **(C)** Height profile of the temperature sensor.
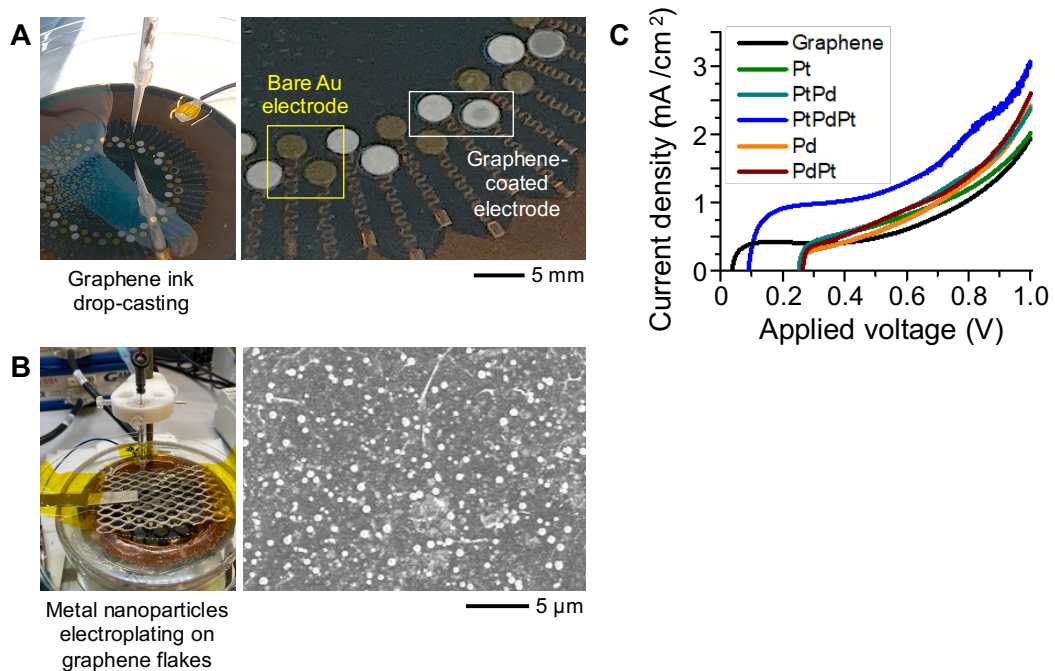
Fig. S10. Development of thin-film glucose sensors. **(A)** Drop-coating of graphene-dispersed solution on bare Au electrodes. **(B)** PtPdPt nanoparticles deposition on the graphene sheets. **(C)** Linear sweep voltammetry obtained from different structures containing Pt and Pd nanoparticles on graphene flakes.
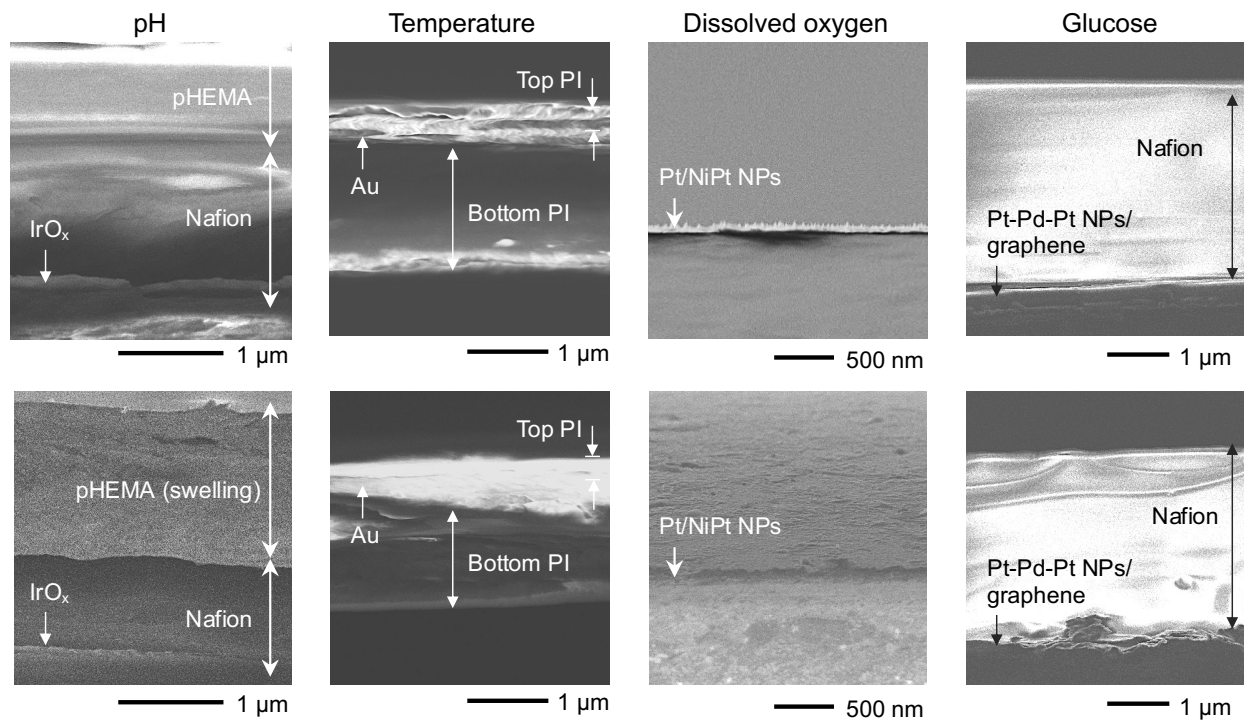
Fig. S11. Cross-sectional SEM images of temperature, pH, glucose, and oxygen sensors. After 7 days of immersion test, the bottom row of the images was obtained.
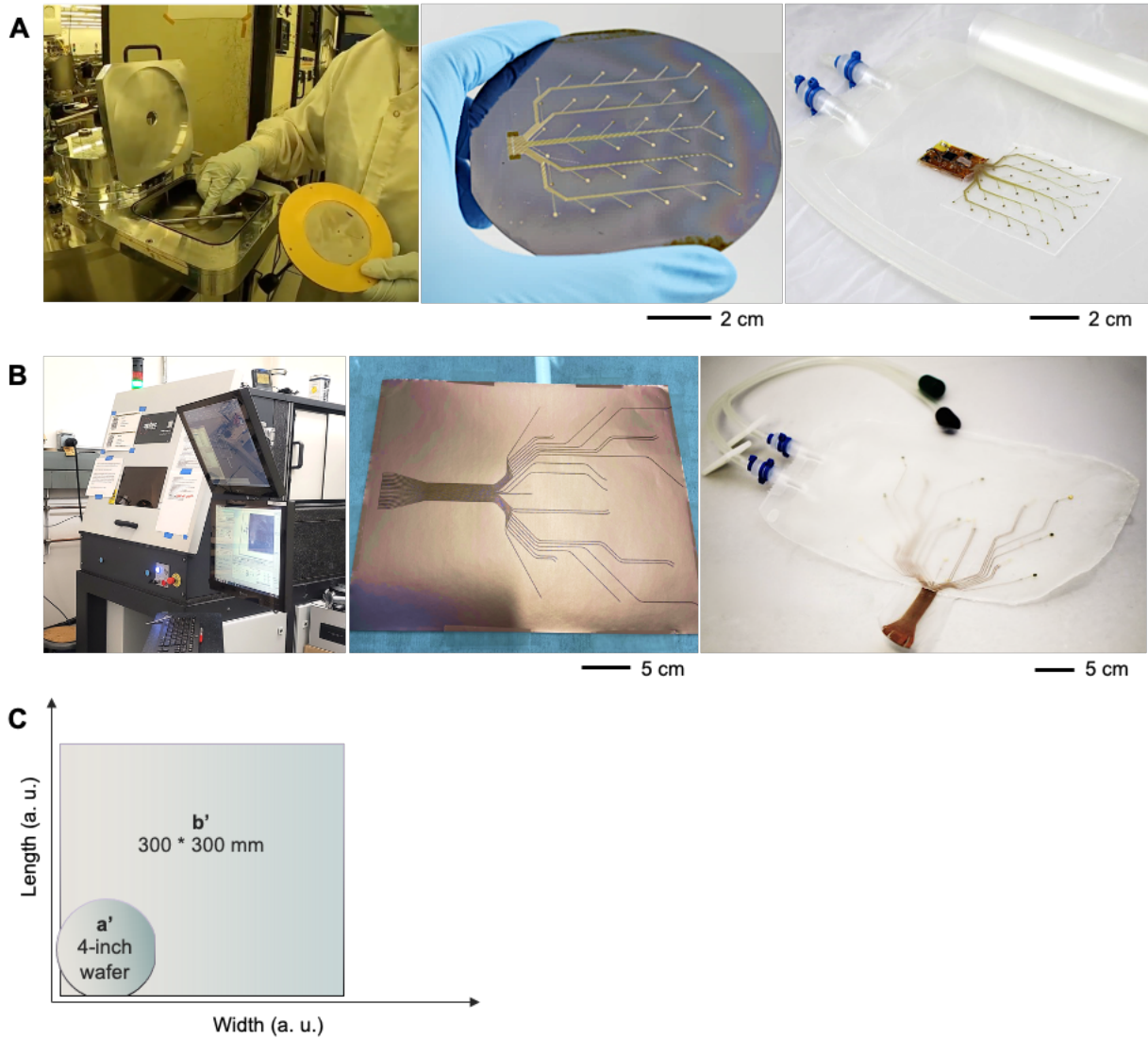
Fig. S12. Fully assembled sensing system integrated onto the inner surface of a commercially available cell bag (Labtainer BioProcess Container 500 mL, Thermo Scientific). The sensor array was prepared through **(A)** cleanroom process (e.g., micropatterning, photolithography) and **(B)** laser-cutting process. **(C)** shows a comparison of maximum preparable array dimensions from each process.

Wireless circuit and sensing system
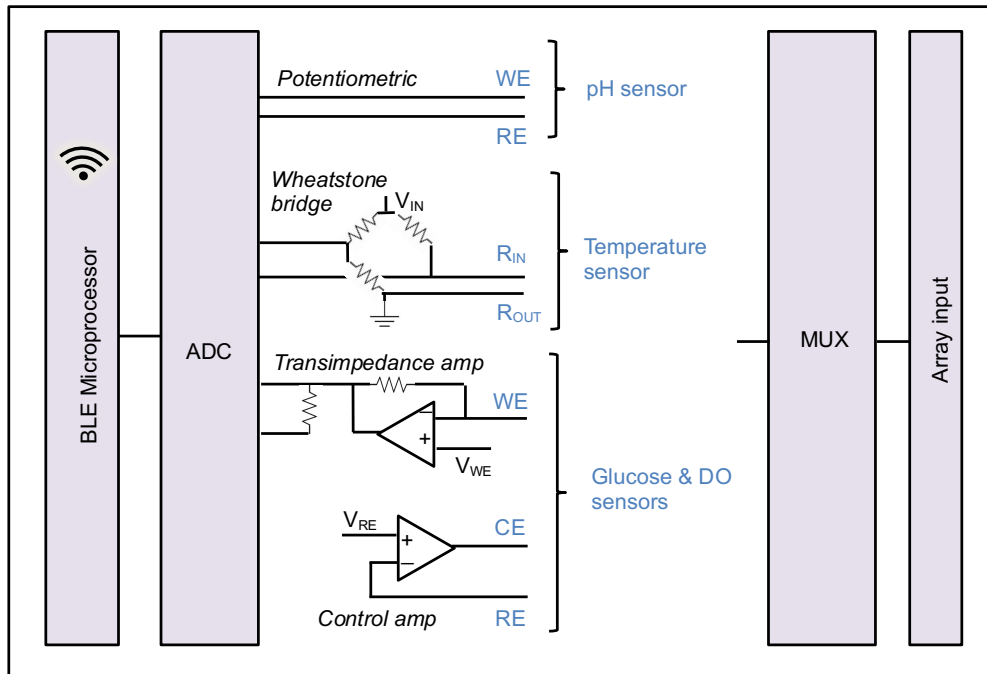
Fig. S13. Schematics of wireless system and sensing circuitry.
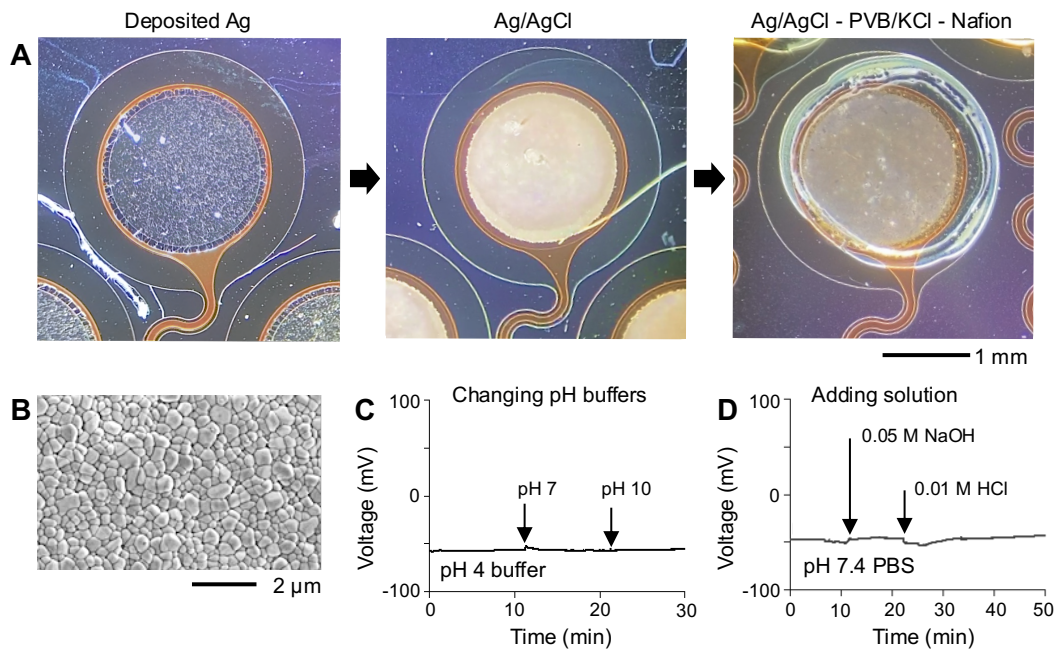
Fig. S14. Fabrication and performance evaluation of thin-film reference electrode. (A) Photographs of the fabrication steps: (1) Ag layer deposited on bare Au electrode, (2) AgCl layer introduced by cyclic chlorination, (3) PVB-KCl and Nafion coating. **(B)** FE-SEM micrograph of the surface of the Ag/AgCl layer (Top-view). Stability evaluation in **(C)** different pH buffers and **(D)** media.
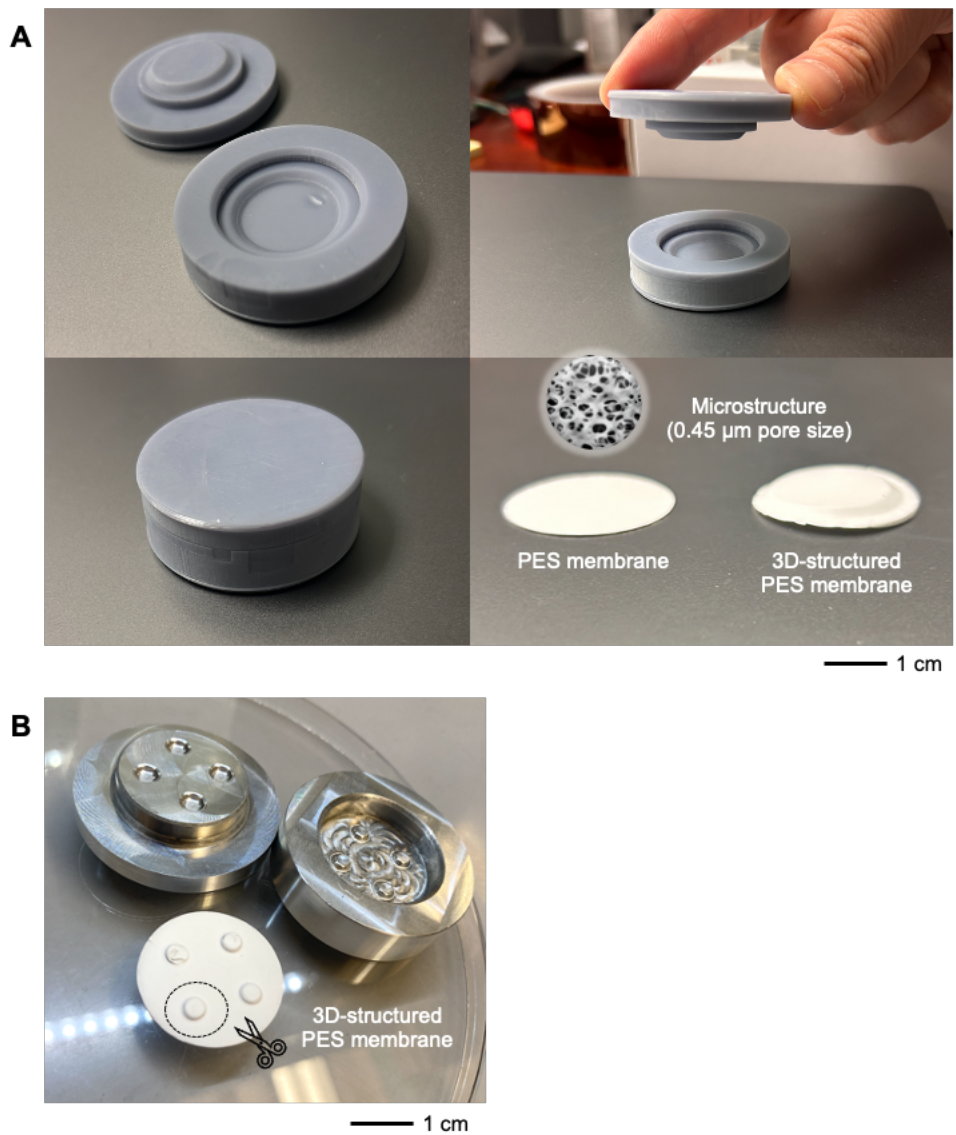
Fig. S15. Customized 3D-printed mold for 3D-structured membrane transformation.
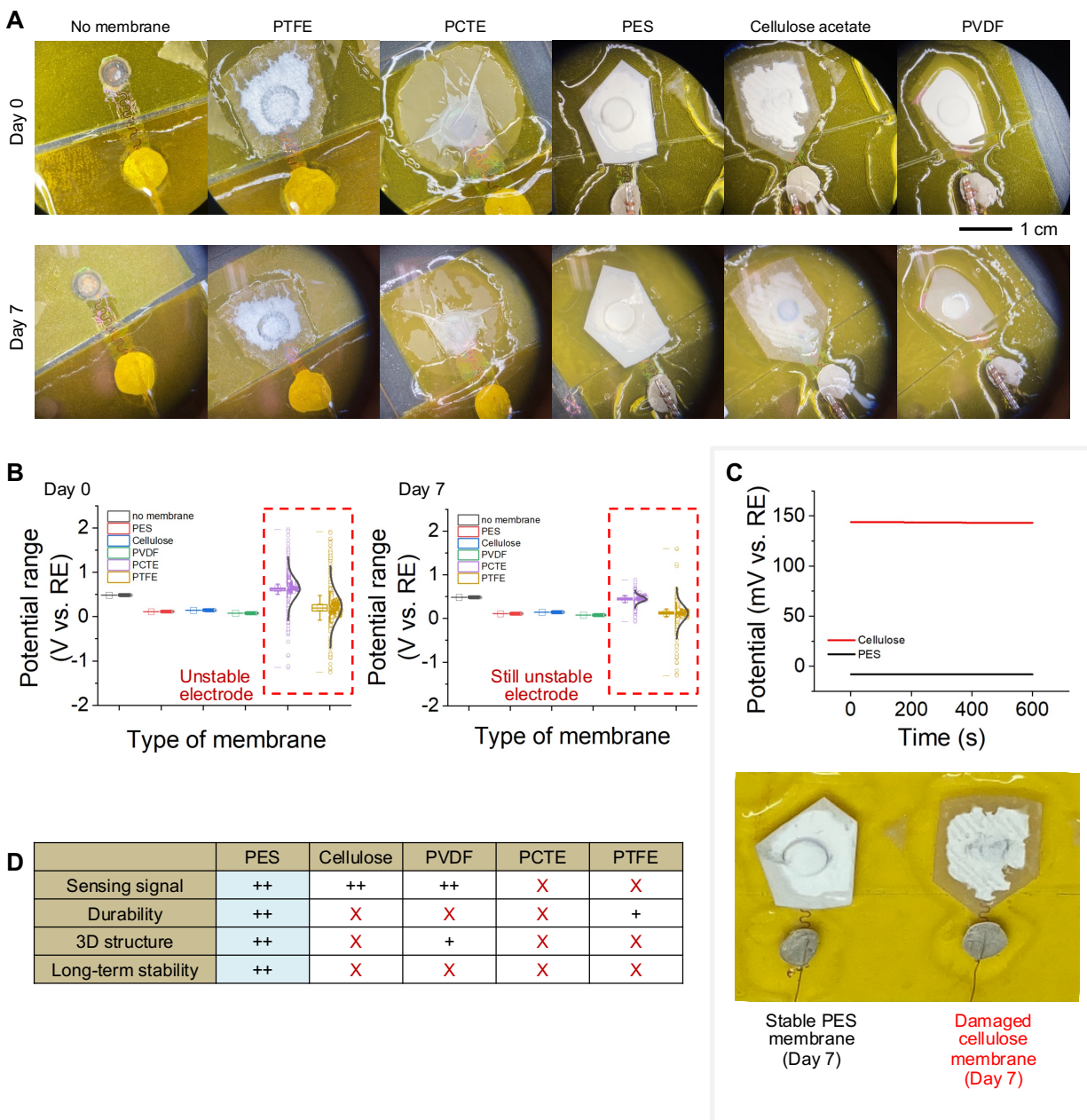
Fig. S16. Effect of different transwell membranes on sensor performance for optimizing sensor preparation. (A) As-prepared pH sensors covered with different transwell membranes. During 7 days, those sensors were fully immersed in the solution and after then their voltage response, durability, and long-term stability were evaluated. **(B)** pH sensor response with different transwell membrane applied (Day 0 and Day 7). **(C)** Day 7 results obtained from the pH sensors covered with PES membrane and cellulose acetate membrane, respectively. The voltage responses of both sensors were well stable, while it turned out that the cellulose acetate membrane couldn't keep its 3D structure as it directly touched the surface of pH sensor. **(D)** Summary of the transwell membrane effect.
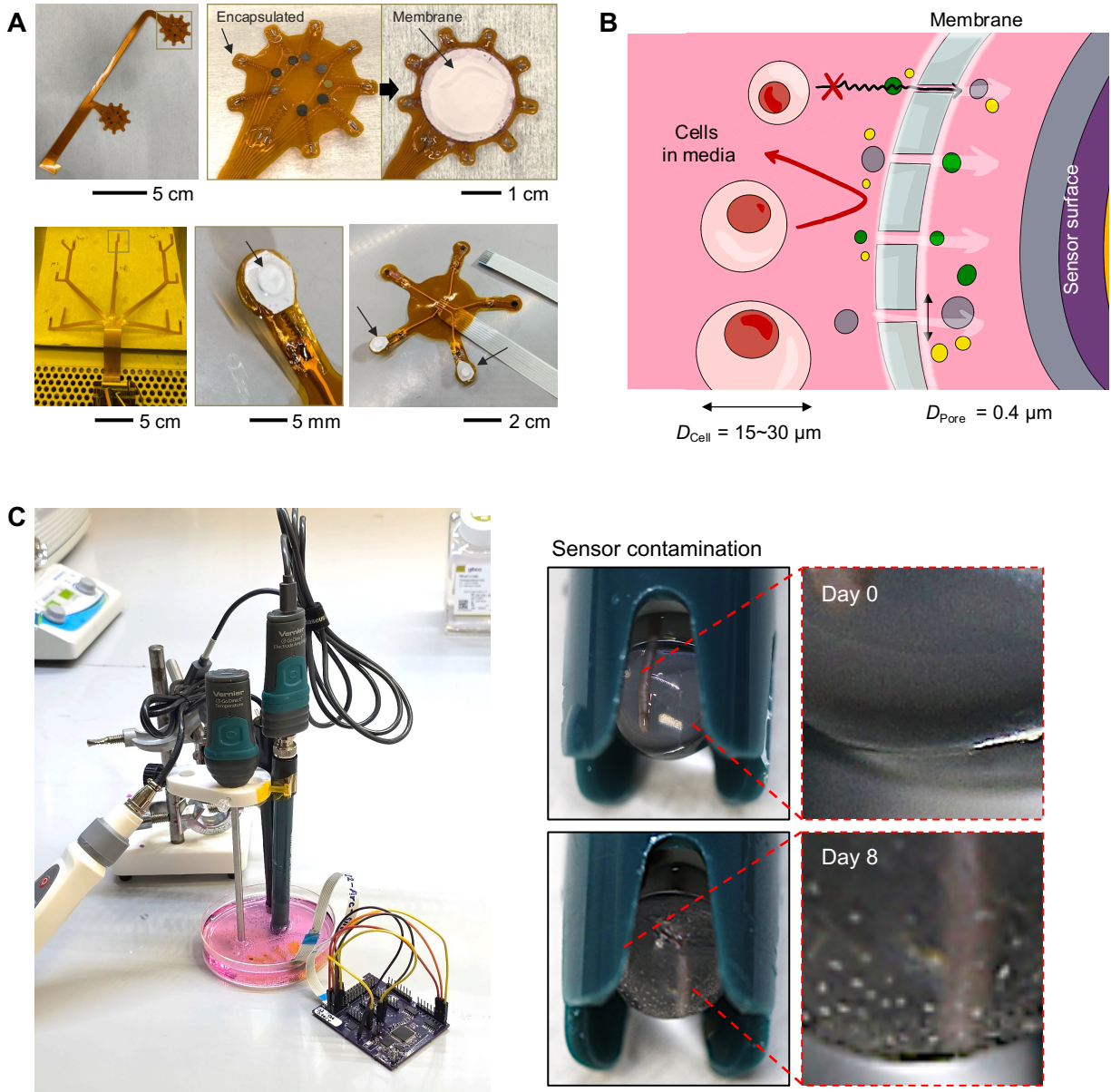
Fig. S17. Sensing platform covered with a PES membrane. (A) Photographs of the fully covered sensor assembly and an individual sensor are presented. **(B)** Scheme of selective filtration process in the media. The submicron pore size of the PES membrane allows small molecules such as ions and water to penetrate, enabling them to directly react on the sensor surface. At the same time, the membrane acts as a barrier, preventing the invasion of stem cells and larger molecules that could potentially cause contamination or deterioration of sensor performance. **(C)** shows a comparison between commercial sensing probes and our wireless sensing assembly. It is important to note that the supertanent or anchoring stem cells present in the media can be adsorbed on the surface of the probes or sensors, leading to contamination concerns.
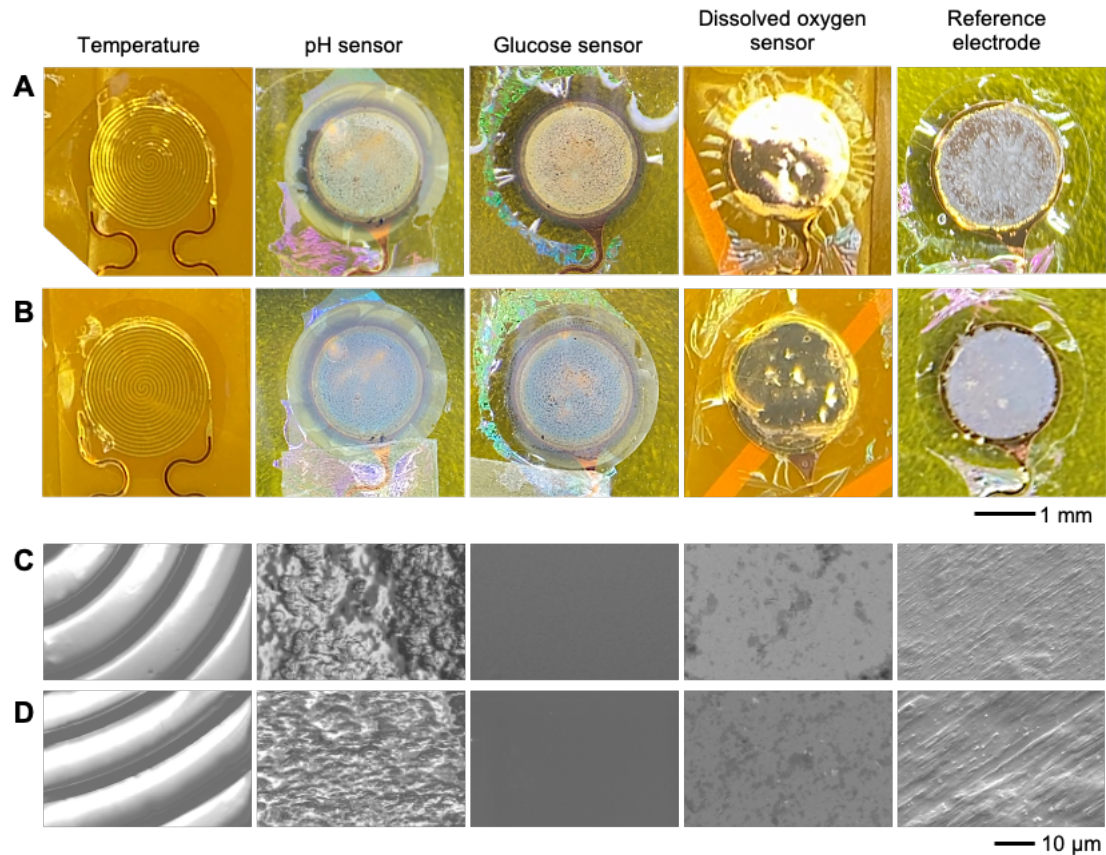
Fig. S18. Optical micrographs and corresponding FE-SEM micrographs of the integrated sensors submerged in a cell-free media before and after a continuous rocking test. (A, C) Surface conditions of the five different electrodes at the beginning of the test. **(B, D)** Surface conditions of the electrodes after 7 days of continuous rocking test under the cell-free media. No observable changes are present.
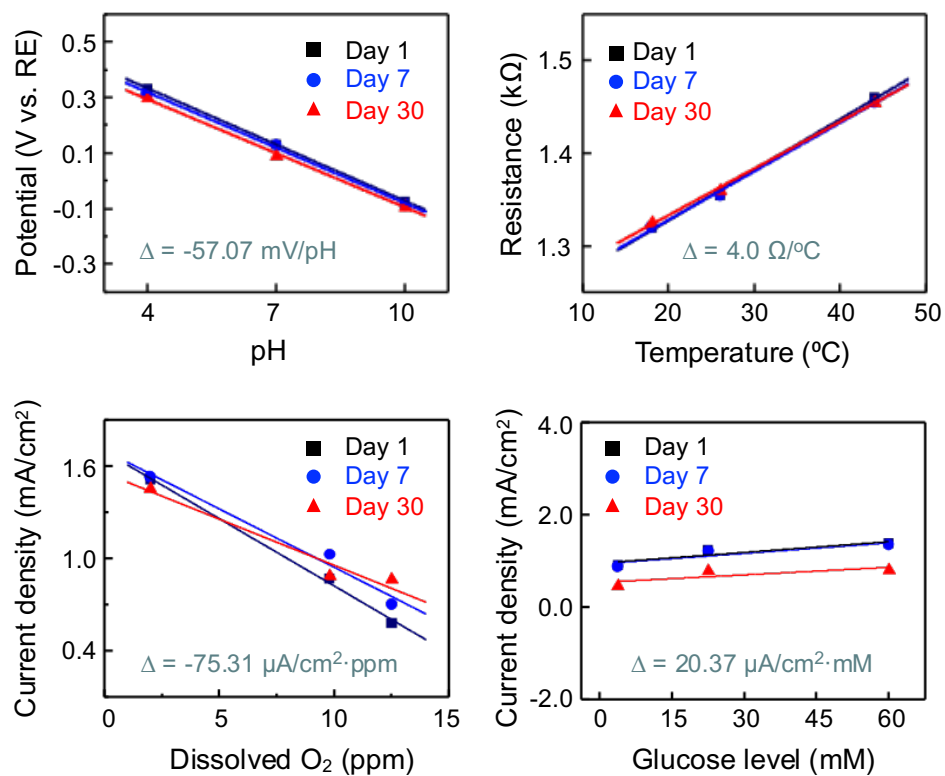
Fig. S19. Long-term stability measurement of pH, temperature, dissolved oxygen (O₂), and glucose sensors during continuous rocking in cell-free media for 30 days.
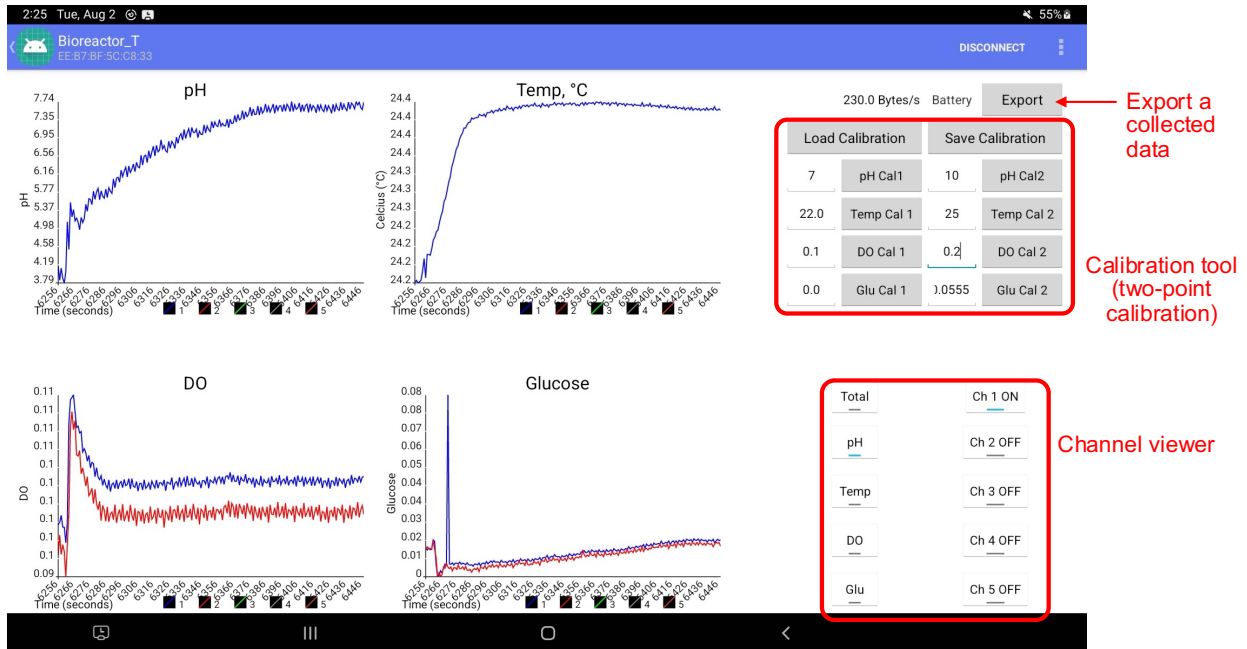
Fig. S20. User interface of the sensor data monitoring application. It displays dedicated monitoring windows for pH, temperature, dissolved oxygen, and glucose on the left panel. The right panel houses the main functionality and features of the application.
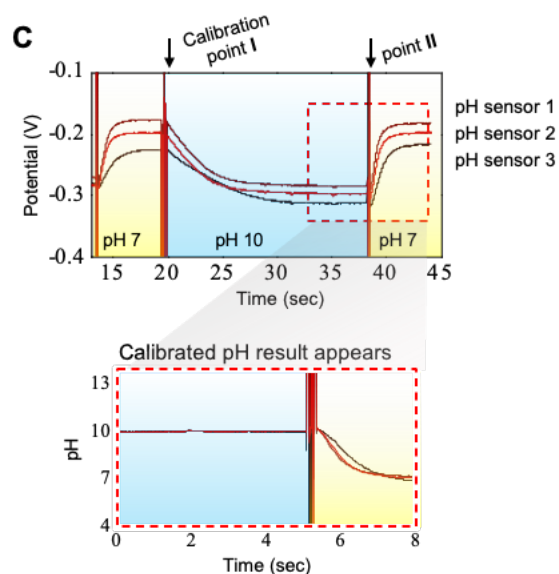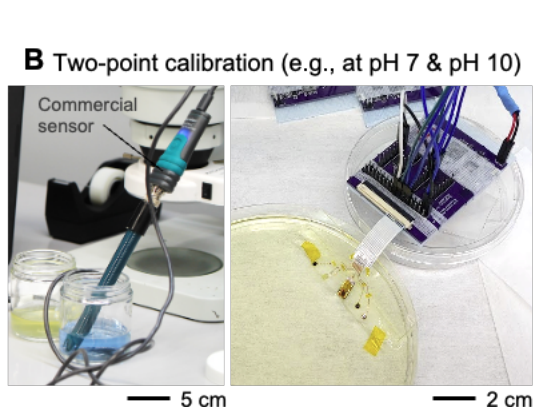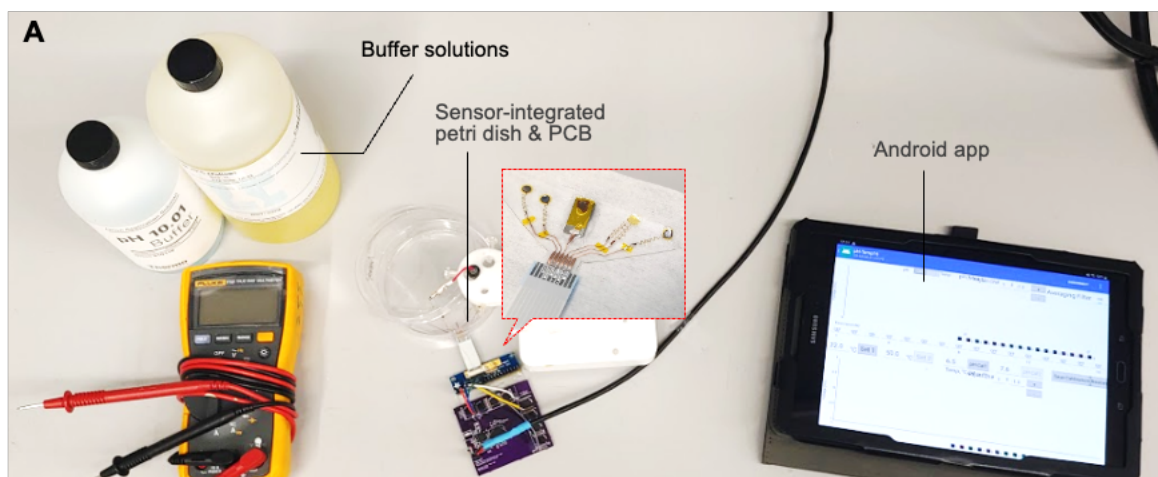
Fig. S21. Overview of two-point pH sensor calibration procedure. (A) Components involved in the calibration process, including two different pH buffer solutions, an electronics-integrated Petri dish, and customized Android app. **(B)** Cross-validation performed using a commercial pH sensor. **(C)** Monitoring result obtained from the calibration process.
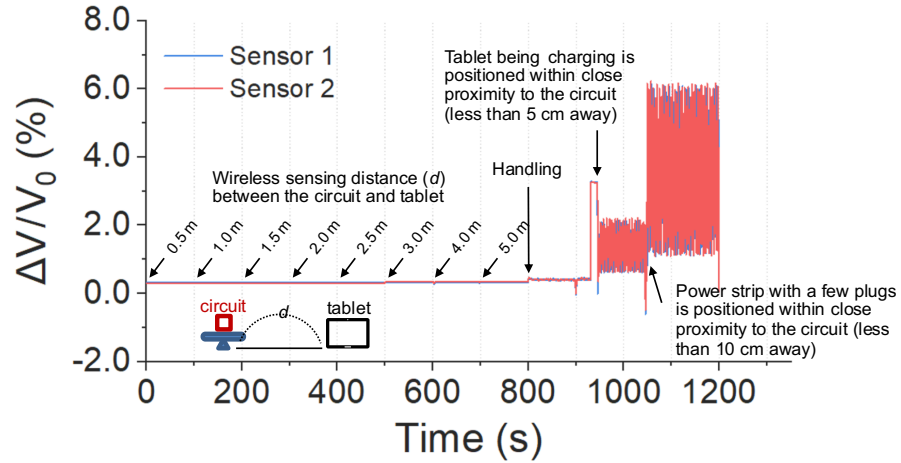
Fig. S22. Signal processing and transfer across varying wireless sensing distances between a wireless circuit and a tablet, ranging from less than 10 cm to 5 m. Considering the potential impact of electricity interference from external circumstances, the wireless circuit is not allowed to be strategically positioned near outlets or in proximity to electrical devices.
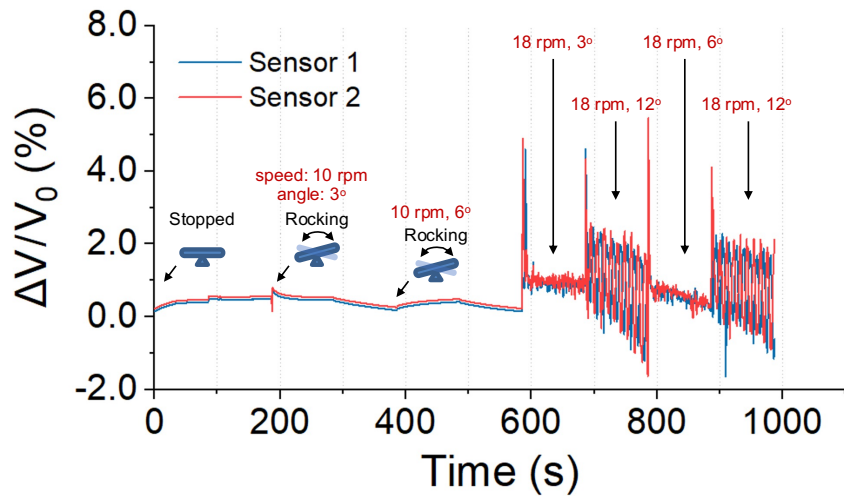
Fig. S23. Induced background noise level in signal resulting from a rocking motion effect.
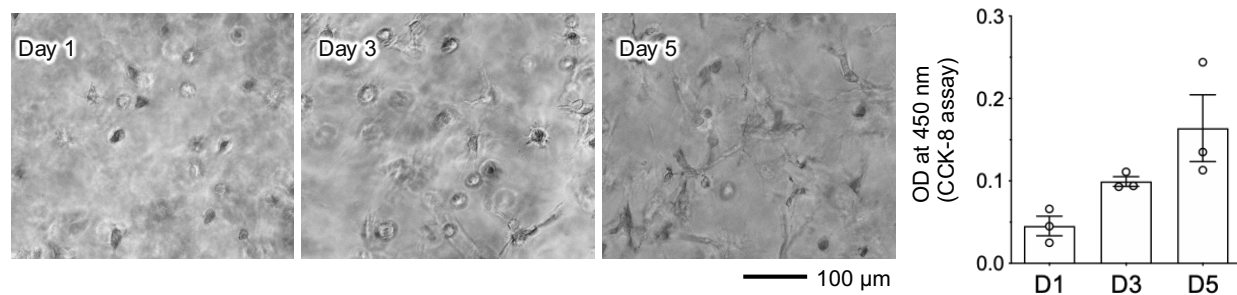
Fig. S24. Time-course morphological change and cellular growth of hMSCs within a gelatin hydroxyphenyl propionic acid hydrogel (GH) matrix cultivated in a bioreactor.
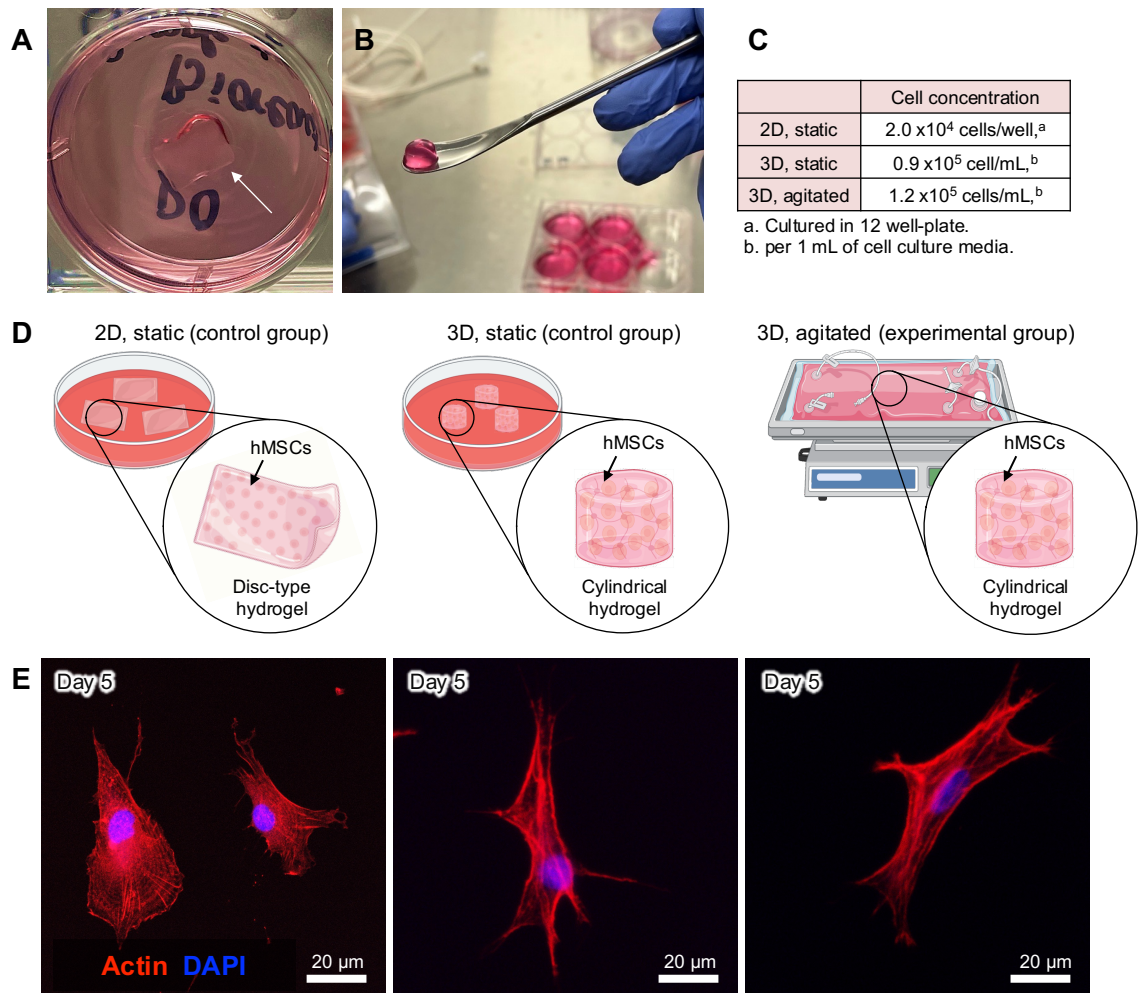
Fig. S25. Cell morphology of hMSCs in 2D and 3D culture. (A) Photos of cell-laden 2D disk-shaped GH hydrogel. **(B)** Photos of cell-encapsulated 3D GH hydrogel. **(C)** Experimental design for 2D and 3D culture in conventional incubator (static) and bioreactor (dynamic). **(D)** Schematic illustration of each cultivation condition. **(E)** Fluorescence cell morphology images of the harvested cells.
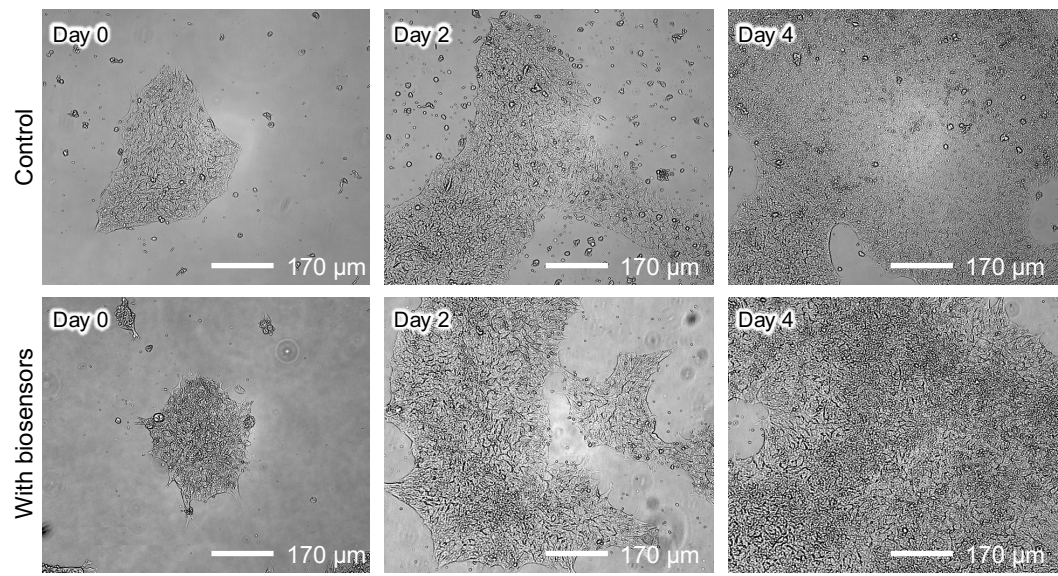
Fig. S26. Time-course morphological change and cellular growth of iPSCs cultivated in an incubator.
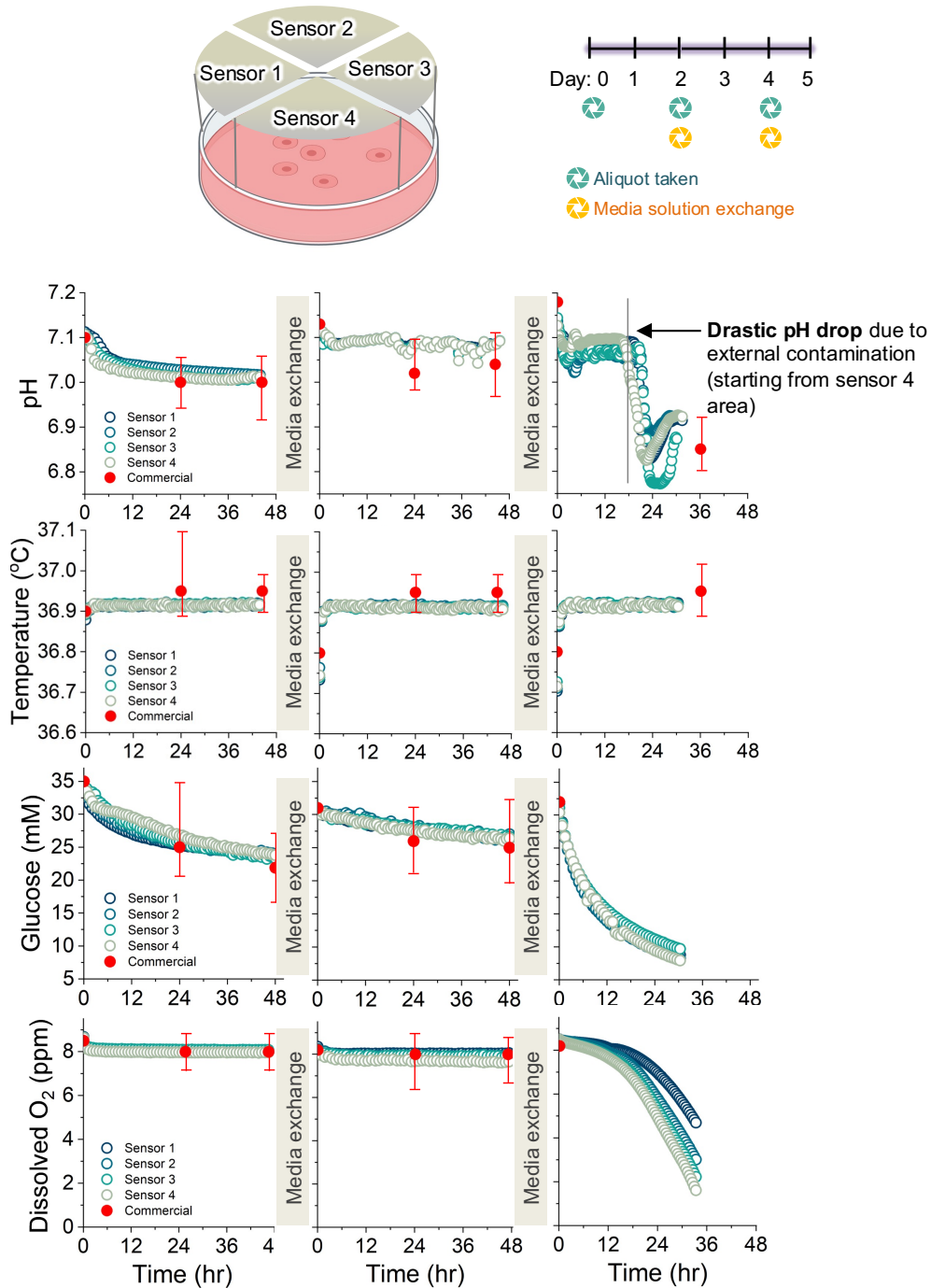
Fig. S27. Monitoring results of iPSCs cultivation over a period of 5 days, with a sampling rate of 1 Hz. Continuously recorded data accompanied by error bars. The fresh media was exchange every other day.
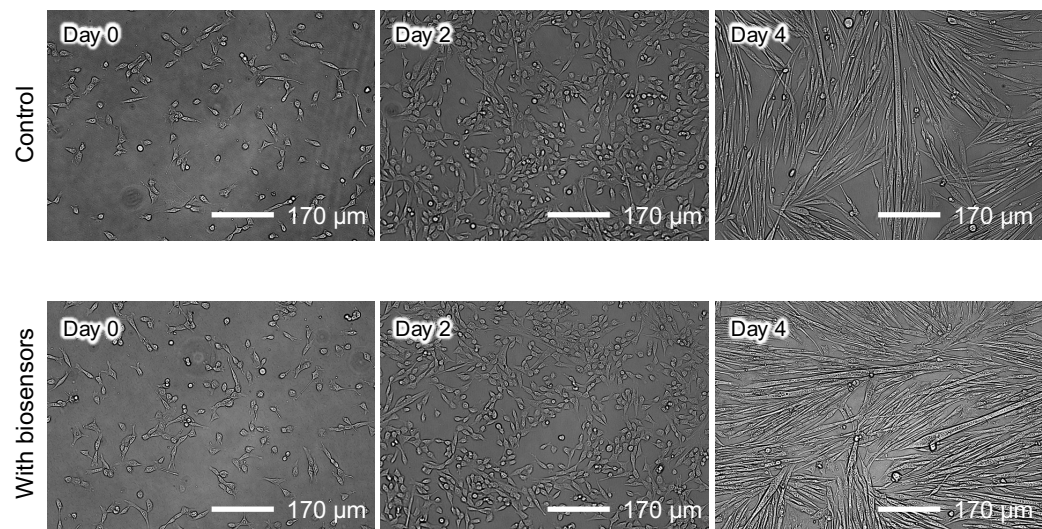
Fig. S28. **Time-course morphological change and cellular growth of mouse primary myoblasts cultivated in an incubator.**
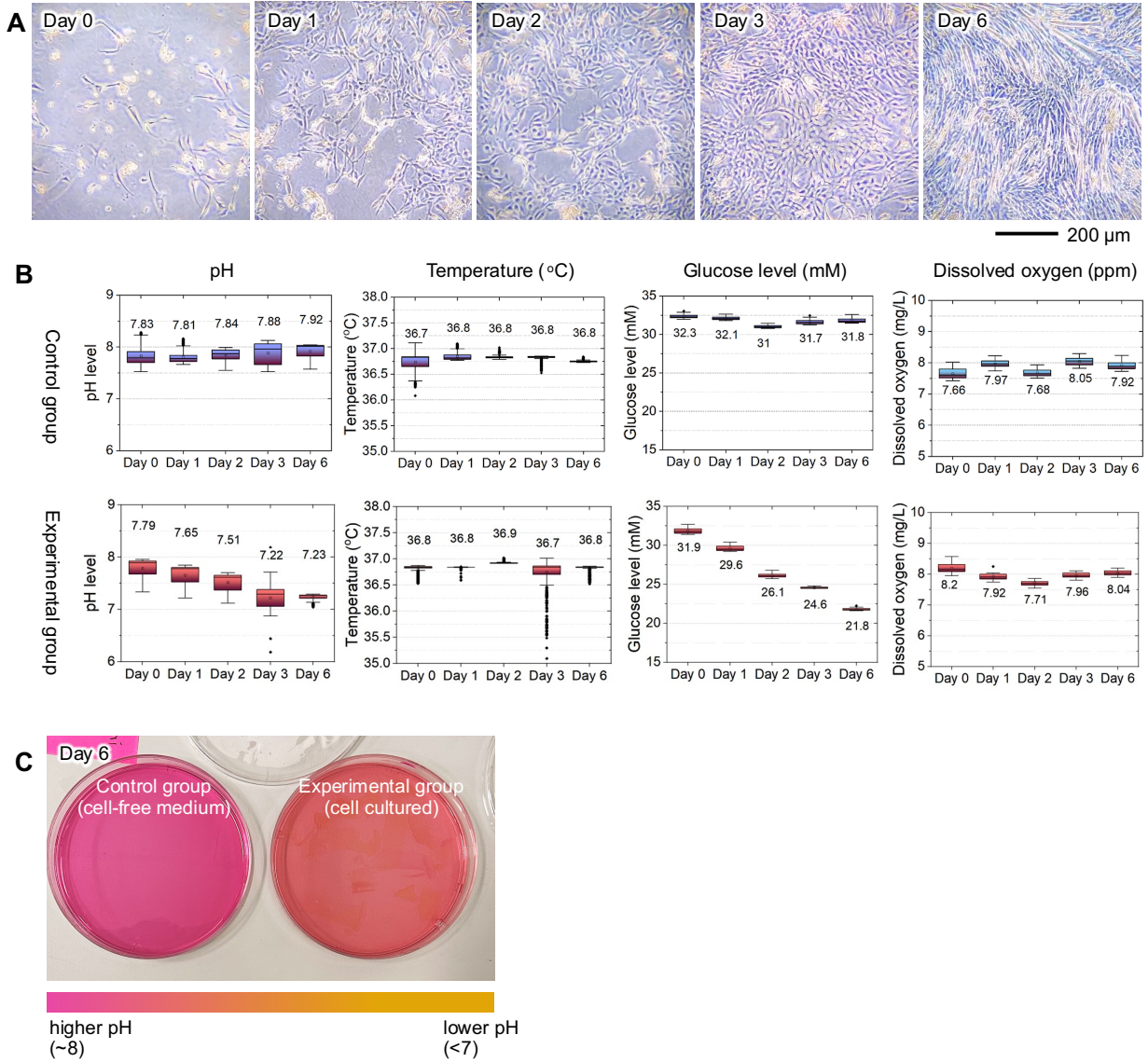
Fig. S29. Monitoring results of C2C12 cultivation over a period of 6 days, with a sampling rate of 1 Hz. (A) Optical images of the cultured cells collected on Days 0, 1, 2, 3, and 6, respectively. **(B)** Continuously recorded data presented using box plots accompanied by error bars. The top row of the data represents the monitoring results of cell-free media, while the bottom row shows the resulrs of C2C12 culture. **(C)** Distinct color difference between the cell-free media and C2C12 media collected on Day 6.
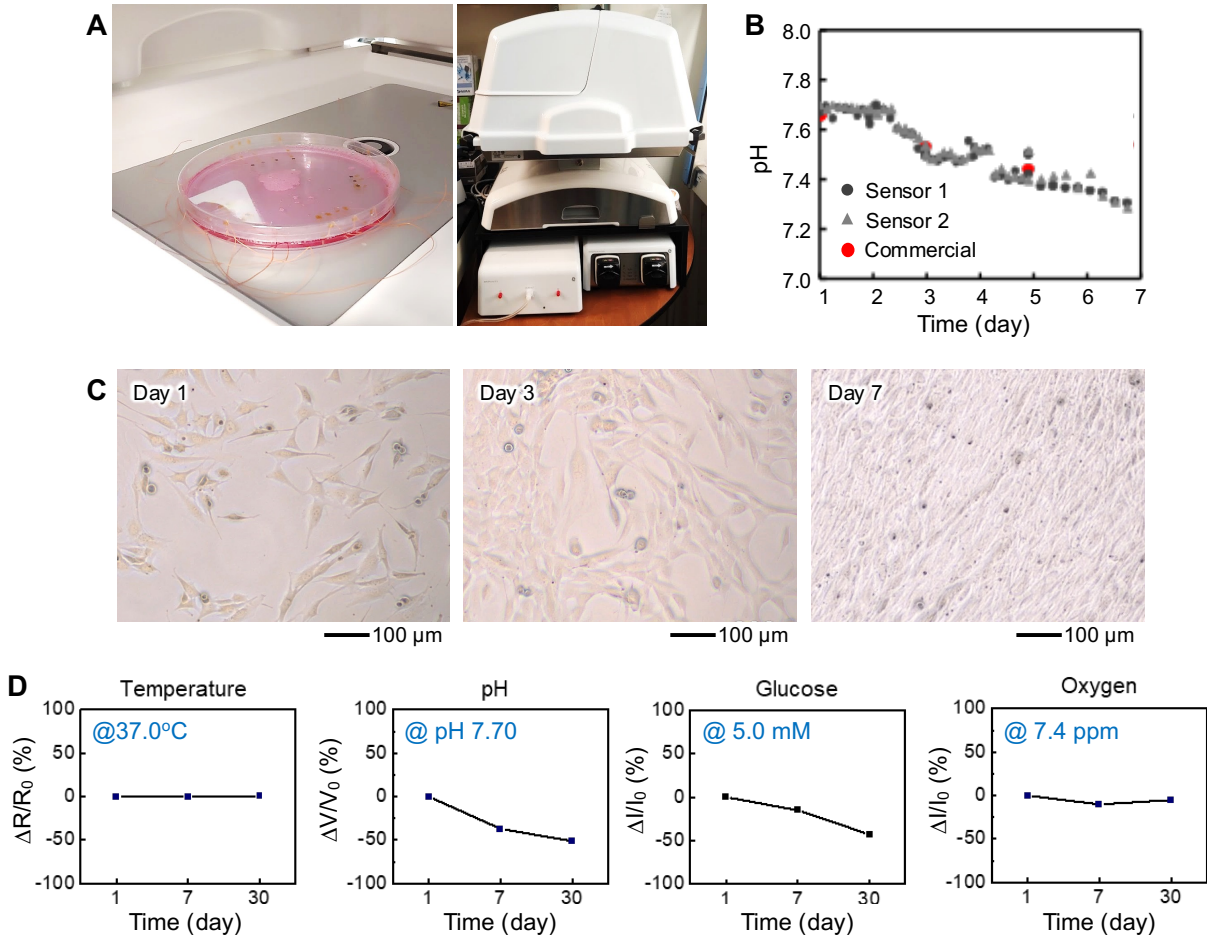
Fig. S30. Long-term monitoring of mouse MSC (mMSCs) culture environment using pH, temperature, dissolved oxygen, and glucose sensors. (A) Photograph of rocking incubator and the thin-film sensors integrated Polystyrene Petri dish that contain mMSC media placed in the incubator. **(B)** Monitoring of pH variation of mMSCs for 7 days. The signal from two thin-film sensors show a similar trend compared to a commercial sensor. **(C)** Microscope images of mMSCs after 1, 3 and 7 days of cultivation. **(D)** Summary of sensing results for 30 days of culture monitoring using thin-film sensors including pH, temperature, dissolved oxygen, and glucose sensors. Each value in the graphs indicates the initial value (Day 0) of the culture environment.
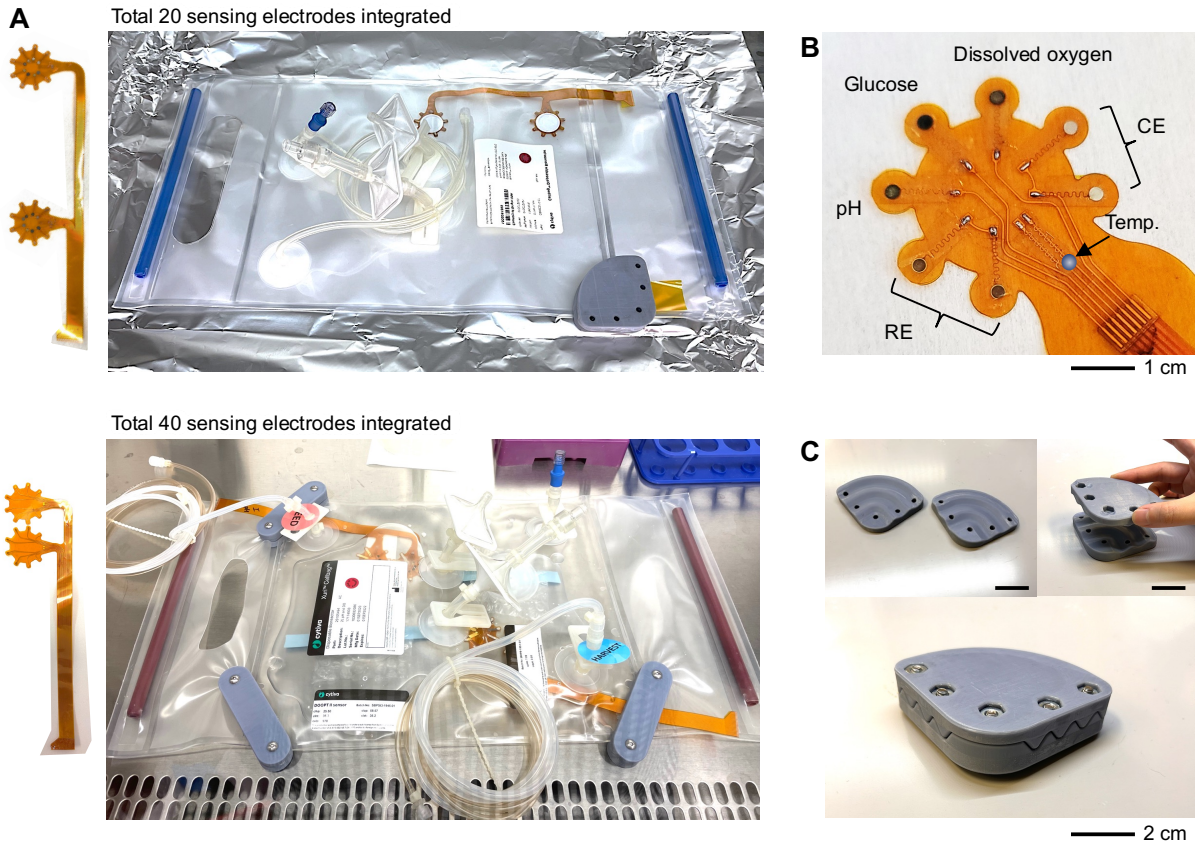
Fig. S31. Wireless electronics-incorporated cell bag. (A) Sensor-integrated cell bag. **(B)** Sensor configuration on an array. **(C)** Custom-made alligator clip for a full sealing the cell bag.
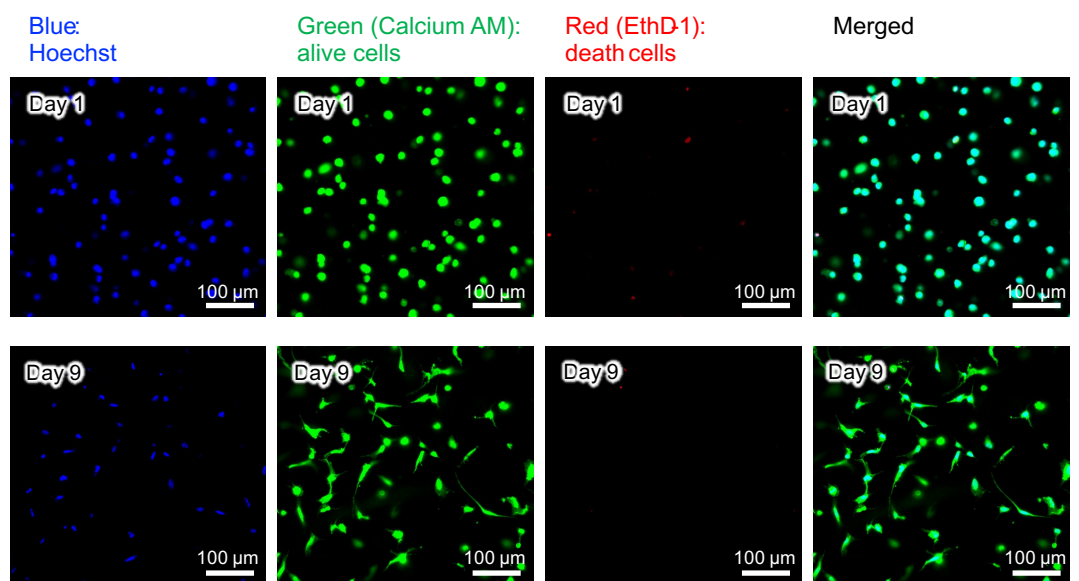
Fig. S32. Fluorescence cell morphology images of the harvested cells. Cells were stained with Hoechst/DAPI to visualize nuclei and ensure they are cells rather than fluorescent debris.
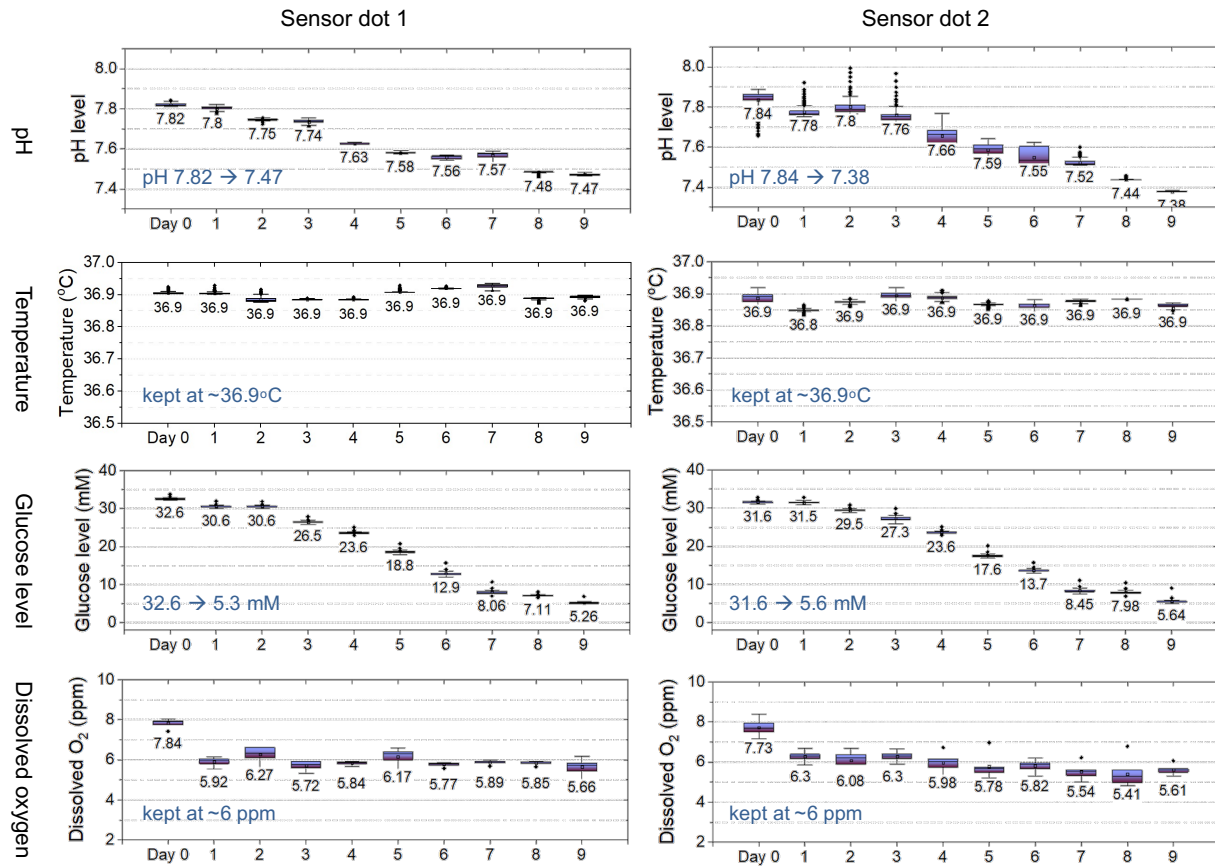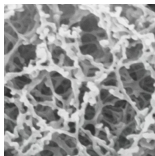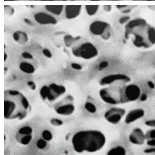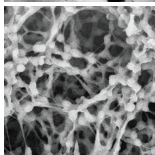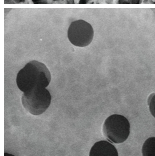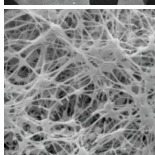
Fig. S33. Monitoring results of hMSC cultivation for a period of 9 days, with a sampling rate of 1 Hz. The continuous data is visually represented using box plots accompanied by error bars.

Table S1. List of key materials comprising main sensors and their mechanical properties.

Type	Materials	Abbreviation	Modulus (MPa)	Max Strain (%)	Poisson ratio	Thickness Range (μm) for simulation
Polymer	Polyimide	PI	2500	4	0.34	1-30
	Polyvinyl butyral	PVB	2	150	0.4	1-300
	poly(2-hydroxyethyl methacrylate)	pHEMA	0.255	181	0.34	1-300
	Nafion	Nafion	249	90	0.3	1-30; 1 (fixed)
	Polydimethylsiloxane	PDMS	0.87	257	0.3	1-20
	Hydrogel	Hydrogel	34.9	500	0.33	1-300
Metallic	Platinum	Pt	168000	0.11	0.5	0.1-3
	Gold	Au	79000	0.26	0.42	0.1-0.6
	Copper	Cu	128000	0.07	0.33	0.7 (fixed)
	Silver	Ag	83000	0.07	0.45	0.2 (fixed)
	Chlorinated silver	AgCl	20000	0.13	0.18	1-4
Metal oxide	Iridium Oxide	IrO_x	194000	0.58	0.4	0.1-15
Composite	Platinum/Palladium/ Platinum-graphene	PtPdPt-Graphene	360000	36	0.39	1-100

Table S2. Comparison of a potential candidate for a hydrophilic transwell membrane, provided by the supplier.

Type	Morphology	Pore size	Thickness	Water flow rate	Young's modulus	Protein binding capacity,[a]	Bacterial Endotoxins
		(μm)	(μm)	$(mL/min \cdot cm^2)$	(GPa)	$(\mu g/cm^2)$	(EU/mL)
Cellulose acetate		0.45	65-110	54.7	1.5-4.0	~20	0.03
Polyethersulfone (PES)		0.45	110-150	58.2	2.5-3.5	5-10	0.001-0.005
Polyvinylidene fluoride (PVDF)		0.45	115	29	2.5-4.0	1-2	<0.03
Polycarbonate (PCTE)		0.60	9	60	2.2-2.4	10-15	0.05-0.15
Polytetrafluoro-ethylene (PTFE)		0.45	25-51	<61	0.5-1.3	0.1-0.2	0.03-0.06

Membrane characteristics were evaluated using the following conditions:

a) Measured using bovine serum albumin (BSA) under static conditions including pH 7.4 and 150 mM NaCl.

Table S3. Simulation results for the calculation of the minimum bending radii of the pH sensor. It is highly desirable to achieve a minimum bending radius below 10 mm (10,000 µm).

pH	Layer 1 (µm) IrO$_x$	Layer 2 (µm) Nafion	Layer 3 (µm) pHEMA	Minimum bending radius (µm)
Job 1	0.1	1	1	38.8
Job 2	5	1	1	39.0
Job 3	10	1	1	28.5
Job 4	15	1	1	30.3
Job 5	0.1	1	100	669.6
Job 6	5	1	100	179.7
Job 7	10	1	100	379.1
Job 8	15	1	100	827.9
Job 9	0.1	1	200	1488.5
Job 10	5	1	200	1821.5
Job 11	10	1	200	1308.3
Job 12	15	1	200	806.9
Job 13	0.1	1	300	1253.9
Job 14	5	1	300	1222.0
Job 15	10	1	300	1172.0
Job 16	15	1	300	1163.0

Table S4. Simulation results for the calculation of the minimum bending radii of the temperature sensor. It is highly desirable to achieve a minimum bending radius below 10 mm (10,000 μm).

Temp.	Layer 1 (μm)	Layer 2 (μm)	Layer 3 (μm)	Minimum bending radius (μm)
	Bottom PI	Au	Top PI	
Job 1	5	0.1	1	659.1
Job 2	5	0.1	10	935.0
Job 3	5	0.1	20	1051.4
Job 4	5	0.1	30	1208.4
Job 5	5	0.2	1	658.8
Job 6	5	0.2	10	934.9
Job 7	5	0.2	20	1051.6
Job 8	5	0.2	30	1207.9
Job 9	5	0.4	1	658.5
Job 10	5	0.4	10	1052.4
Job 11	5	0.4	20	1207.3
Job 12	5	0.4	30	1208.1
Job 13	5	0.6	1	658.5
Job 14	5	0.6	10	935.4
Job 15	5	0.6	20	1052.4
Job 16	5	0.6	30	1208.2

Table S5. Simulation results for the calculation of the minimum bending radii of the dissolved oxygen sensor. It is highly desirable to achieve a minimum bending radius below 10 mm (10,000 µm).

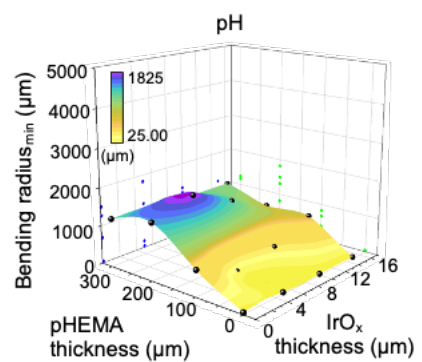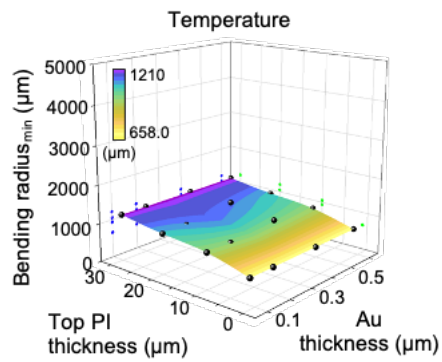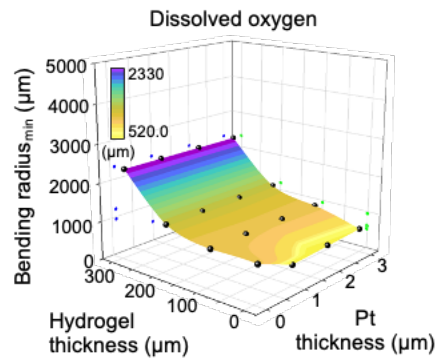| DO	Layer 1 (µm)	Layer 2 (µm)	Layer 3 (µm)	Minimum bending radius (µm)
	Pt	Hydrogel	Nafion	
Job 1	0.1	1	1	941.5
Job 2	0.1	100	1	941.5
Job 3	0.1	200	1	1207.4
Job 4	0.1	300	1	2326.6
Job 5	1	1	1	522.3
Job 6	1	100	1	941.4
Job 7	1	200	1	1207.1
Job 8	1	300	1	2326.4
Job 9	2	1	1	590.8
Job 10	2	100	1	941.3
Job 11	2	200	1	1206.7
Job 12	2	300	1	2326.1
Job 13	3	1	1	619.4
Job 14	3	100	1	941.1
Job 15	3	200	1	1206.2
Job 16	3	300	1	2325.8

Table S6. Simulation results for the calculation of the minimum bending radii of the glucose sensor. It is highly desirable to achieve a minimum bending radius below 10 mm (10,000 μm).

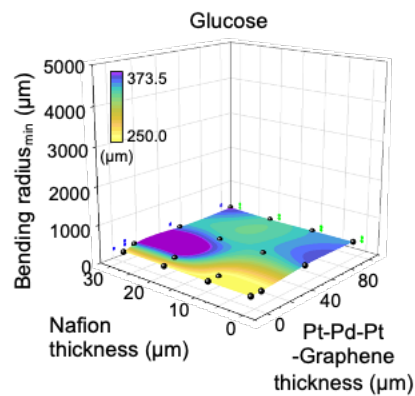| Glucose	Layer 1 (μm) PtPdPt-graphene	Layer 2 (μm) Nafion	Minimum bending radius (μm)
Job 1	1	1	<250.0
Job 2	10	1	<250.0
Job 3	50	1	355.4
Job 4	100	1	353.2
Job 5	1	10	<250.0
Job 6	10	10	<250.0
Job 7	50	10	341.1
Job 8	100	10	347.9
Job 9	1	20	<250.0
Job 10	10	20	348.6
Job 11	50	20	347.5
Job 12	100	20	338.8
Job 13	1	30	<250.0
Job 14	10	30	353.2
Job 15	50	30	353.9
Job 16	100	30	373.1

Table S7. Simulation results for the calculation of the minimum bending radii of the reference electrode. It is highly desirable to achieve a minimum bending radius below 10 mm (10,000 µm).

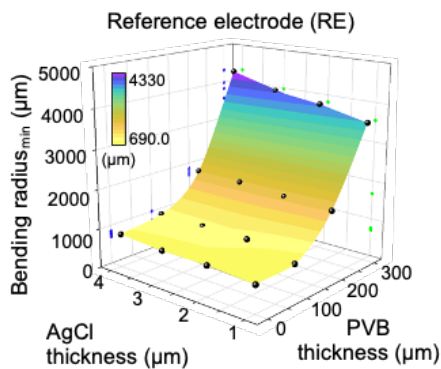| Ref.	Layer 1 (µm)	Layer 2 (µm)	Layer 3 (µm)	Layer 4 (µm)	Minimum bending radius (µm)
	Ag	AgCl	PVB	Nafion	
Job 1	0.2	1	1	1	699.8
Job 2	0.2	1	100	1	750.0
Job 3	0.2	1	200	1	1662.9
Job 4	0.2	1	300	1	3550.8
Job 5	0.2	2	1	1	772.0
Job 6	0.2	2	100	1	1004.4
Job 7	0.2	2	200	1	1718.4
Job 8	0.2	2	300	1	3816.1
Job 9	0.2	3	1	1	771.1
Job 10	0.2	3	100	1	1002.8
Job 11	0.2	3	200	1	1809.8
Job 12	0.2	3	300	1	3977.3
Job 13	0.2	4	1	1	844.0
Job 14	0.2	4	100	1	1001.9
Job 15	0.2	4	200	1	1838.1
Job 16	0.2	4	300	1	4323.8

Reference electrode (RE)

Table S8. Manufacturing cost of the flexible sensor array (based on 4-inch wafer; total 36 sensors available).

Material	Polyimide	PDMS	Au	Cu	Precursor solution (Ir, Pt, Pd, Ni)	Nafion	PES
Component	Sensor and interconnect substrate	Sensor substrate	Sensing electrode	Sensing electrode and interconnect	Active sensing layer	Surface protective layer	Antifouling membrane
Fabrication process	Photolithography	Spin coating	E-beam deposition	E-beam deposition	Electrodeposition	Drop-casting	Commercially available
Material price ($/unit of device)	$0.045	$0.05	$0.35	$0.0034	$0.013	<$0.0001	$0.43625

Total price: ~$0.93/unit

Movie S1. Overview of the Smart Bioreactor system.

Movie S2. Key features of the Smart Bioreactor system.
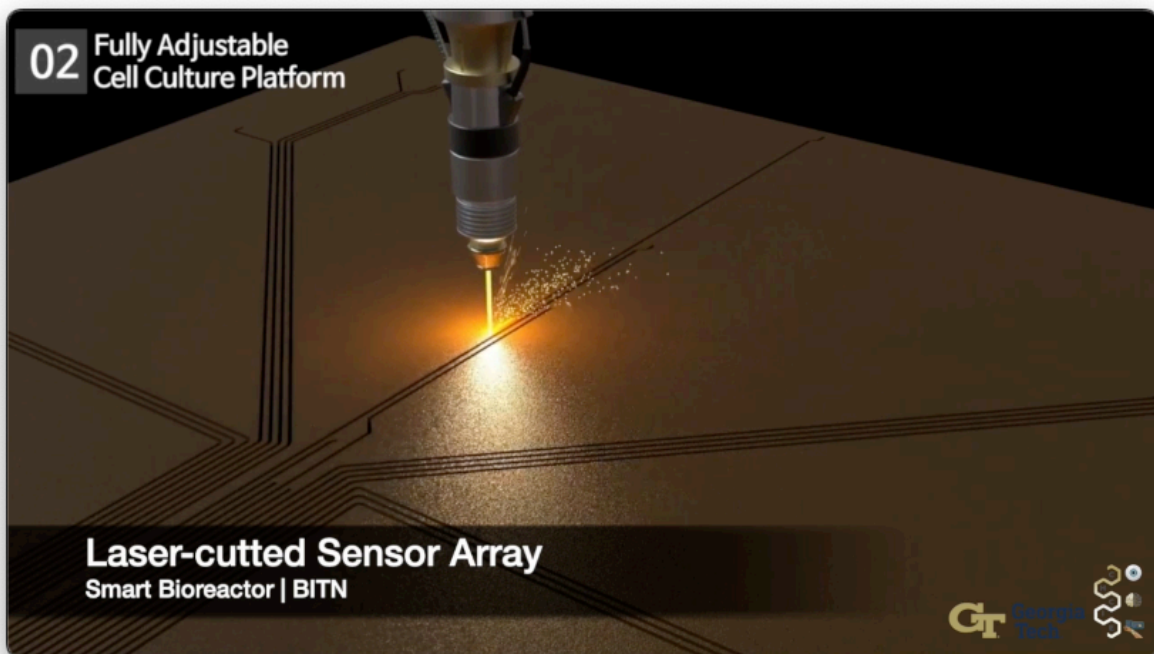
Movie S3. Sensor response upon a change in injected solutions.